NANO LETTERS

Letter

pubs.acs.org/NanoLett

Young's Modulus, Residual Stress, and Crystal Orientation of Doubly Clamped Silicon Nanowire Beams

Y. Calahorra, O. Shtempluck, V. Kotchetkov, and Y. E. Yaish*

Department of Electrical Engineering, Technion, Haifa 32000, Israel

ABSTRACT: Initial or residual stress plays an important role in nanoelectronics. Valley degeneracy in silicon nanowires (SiNWs) is partially lifted due to built-in stresses, and consequently, electron−phonon scattering rate is reduced and device mobility and performance are improved. In this study we use a nonlinear model describing the force-deflection relationship to extract the Young's modulus, the residual stress, and the crystallographic growth orientation of SiNW beams. Measurements were performed on suspended doubly clamped SiNWs subjected to atomic force microscopy (AFM) three-point bending constraints. The nanowires comprised different growth directions and two SiO_2 sheath thicknesses, and underwent different rapid thermal annealing processes. Analysis showed that rapid thermal annealing introduces compressive strains into the SiNWs and may result in buckling of the SiNWs. Furthermore, the core−shell model together with the residual stress analysis accurately describe the Young's modulus of oxide covered SiNWs and the crystal orientation of the measured nanowires.

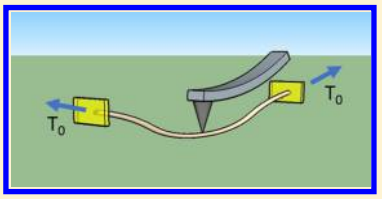

KEYWORDS: *Silicon nanowire, residual tension, atomic force microscopy, crystal orientation*

Over the past decade, silicon nanowires (SiNWs) have attracted a great deal of attention as future building blocks for nanoelectronics. Researchers have described, for example, SiNWs-based electronic devices,[1−3] nanoelectromechanical systems (NEMS),[4−6] and chemical and biological sensors,[7−9] in many of which the mechanical properties of SiNWs play an important role.[10] Moreover, the ability to measure and control the initial stress of electronic devices (sometimes referred to as residual tension when dealing with postprocessing effects) is an important and exciting possibility, due to piezoresistive effects that may improve device performance. Indeed, strain engineering is nowadays used quite extensively in the microelectronics industry.[11−13] In this respect, SiNWs have an unusually large piezoresistive coefficient, as reported by He and Yang,[10] thus increasing the motivation for SiNW strain engineering applications. Understanding the mechanical properties of SiNWs and being able to quantify and control them, are of crucial importance for successful realization of such applications.

Different measurement schemes have been introduced to study the physical and mechanical properties of SiNWs, including scanning (SEM) and transmission electron microscopy (TEM),[14−20] nanoindentation techniques,[21,22] dynamic resonance measurements,[4,23] and atomic force microscopy (AFM) based three-point bending measurement setup.[23−34] The advantage offered by the last two methods is the ability to perform measurements directly on fabricated devices, such as doubly clamped SiNW beams, thus taking process influences into consideration.

A doubly clamped beam may develop residual stresses during clamping or due to subsequent processing, or may accommodate an inherent initial stress all of which can affect its electronic properties. In this study, a new approach is introduced for the analysis of three-point bending experiments of doubly clamped SiNW beams taking initial stress into account. This method enables us to accurately extract the NW's Young's modulus and the wire crystallographic growth orientation. This unique postprocessing characterization enables to extract relevant wire parameters even after device fabrication has been completed.

Doubly clamped suspended SiNW beams were fabricated in a single step e-beam lithography (EBL) process discussed elsewhere.[35] SiNWs were deposited upon a sacrificial PMMA layer (MicroChem), spin-coated on a 100 nm Si_3N_4 passivated Si wafer. Two subsequent PMMA layers, corresponding to a standard EBL lift-off process, were spin coated on the SiNW bearing die. The SiNWs were optically located, and EBL was used to define anchoring electrodes. The die was then placed in a high-vacuum e-gun evaporation system, and evaporation was carried out using a homemade rotating tilted stage to achieve better encapsulation of the SiNW within the metal; circumferential embedding of the SiNW has been noted as a key factor for better elastic response of the studied system.[36] NiCr/Au source and drain electrodes were deposited until the NW was embedded within the two constraints. The encapsulation of the SiNWs between the two PMMA layers and the circumference metallic anchoring contacts were essential for providing untwisted deformation of the studied wires and negligible shear strains throughout the three-point bending experiments.

Three-point bending experiments were carried out within a DI-Veeco Nanoscope V AFM system in a Nanoman environment that allows control of tip oscillation and 3-D position. Figure 1 shows a schematic description of the AFM-based three-point bending experiment. Figure 1a,b corresponds to a typical SiNW before and after bending, respectively.

Received: December 14, 2014
Revised: March 17, 2015

 © XXXX American Chemical Society

DOI: 10.1021/nl5047939
Nano Lett. XXXX, XXX, XXX−XXX

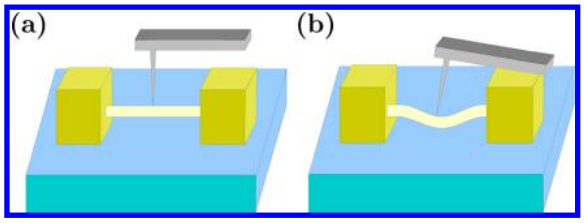

Figure 1. Schematic diagram of the SiNW beam, clamped by an embedding metallic contact, subjected to a point force applied by an AFM tip. (a) The beam prior to bending. (b) The beam during bending test. The total descent, z_{piezo}, is the sum of the NW deflection, z_{SiNW}, and the cantilever deflection, $z_{cantilever}$.

Prior to the bending tests, devices were carefully imaged by AFM tapping mode, to verify the beam shapes and to identify the axial center point. The transversal center point was found within the Nanoman environment and is the highest point during a transversal pass over the NW with drive and feedback on. The vertical deflection of the NW was recorded during the undriven piezoelectric controlled descent of the tip to the NW. The total descent, generated by the piezoelectric crystal, is divided between the deflections of the device and the AFM cantilever

$$z_{piezo} = z_{SiNW} + z_{cantilever} \quad (1)$$

where z_{piezo} and $z_{cantilever}$ are measured quantities, thus allowing the extraction of the device's deflection, z_{SiNW}. The AFM cantilever obeys Hook's law, $F_{applied} = z_{cantilever} \cdot k_{cantilever}$, so a single measurement yields the force–deflection (F–D) curve. Since the AFM's output signals are electronic voltages, calibration is performed on a hard substrate to transform the raw cantilever deflection data into distance units. The bending tests were repeated several times for each device with reproducible results, showing the rigidity of the constraints, and the elastic nature of the devices within the measured range.

Rapid thermal annealing (RTA) was performed in a dedicated furnace; the process includes heating the post-fabrication die to 300–400 °C in a forming gas atmosphere. Several devices were measured before and after RTA, and the mechanical influence of RTA was examined. Figure 2a,b shows TEM images of unoxidized and oxidized SiNWs, respectively.

The different SiO_2 sheath thickness is clearly discernible. Thicknesses of 2 and 7 nm were used to calculate E_{Si} from the resulting E_{eff} using eq 14, depending on the NWs used for device fabrication.

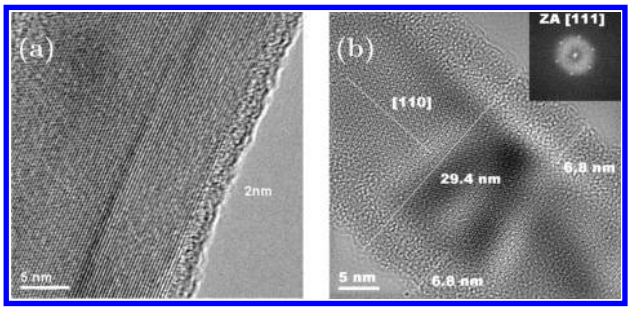

Figure 2. (a) TEM image of a SiNW taken from the same wafer made for device fabrication. A native SiO_2 sheath of about 2 nm is clearly visible. (b) TEM image of a thermally oxidized SiNW. The SiO_2 layer is usually about 7–8 nm thick. The inset shows the diffraction pattern taken from the NW core, showing the ⟨111⟩ zone axis.

Figure 3 depicts a typical measured F–D curve and two fitting curves, obtained by the analytical model discussed

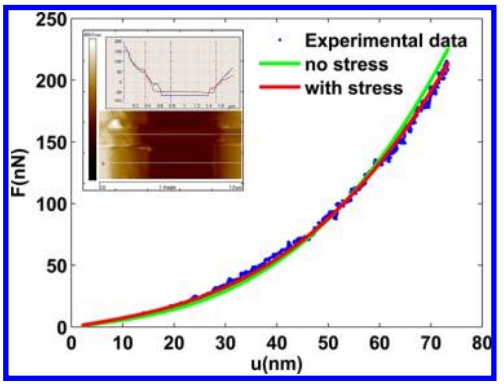

Figure 3. Measured F–D curve (blue dots) and fitted curves according to the analytical model with and without initial stress (red and green curves, respectively). The extracted parameters are E_{eff} = 140 GPa, σ_0 = 96 MPa, and E_{eff} = 160 GPa for fitting with/without initial stress, respectively. Inset shows an AFM topography image of two cross section lines taken from the suspended NW (red) and substrate surface (blue).

shortly. The beam's diameter and length are extracted from the AFM measurements. The inset presents two cross sections taken from the topography image showing the substrate region and the suspended device. Measurements were also performed on similar devices before and after RTA. Nickel-silicide has been used to improve metal/semiconductor contacts in SiNW devices.[37–39] At temperatures of 300–500 °C, Ni atoms diffuse into the SiNW creating various Ni-silicide compounds.[40,41] The silicidation process creates compressive strains along the SiNW, as confirmed by TEM measurements.[16] Hence, devices are expected to have smaller initial stress values after RTA; indeed, values may even be negative.

Figure 4 shows measured F–D curves taken from the same device before and after RTA at 400 °C for 30 s. In other cases,

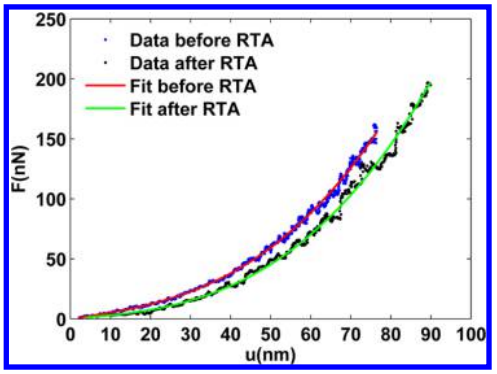

Figure 4. Measured F–D curve (blue and black dots) and fitting curves (red and green lines) for a SiNW before and after RTA at 400 °C. Fitting results before RTA, E_{eff} = 123 GPa and σ_0 = 159 MPa, and after RTA, E_{eff} = 113 GPa and σ_0 = 45 MPa.

devices altered their geometry following RTA to yield an arched beam, implying buckling due to axial compression. Figure 5a presents a typical SEM image of a horizontal beam used in the reported experiments; Figure 5b shows an arched beam resulting from the same beam after RTA. The mechanical properties of arched beams differ from those of horizontal beams and will be discussed in a separate publication.[42]

DOI: 10.1021/nl5047939
Nano Lett. XXXX, XXX, XXX–XXX

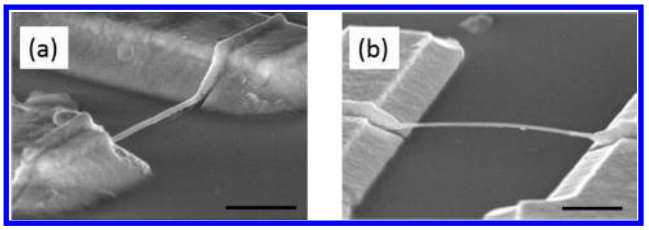

Figure 5. SEM images of a horizontal SiNW beam (a) and an arched beam (b). Arched beams have a characteristic F−D curve that is significantly different from that of horizontal beams. Scale bar − 0.5 μm.

To extract the relevant NW parameters, such as Young's modulus, residual tension, and crystallographic growth orientation, an analytical model for the three-point bending experiment is developed. The starting point is the basic differential equation of continuous mechanics that determines the equilibrium position of a doubly clamped beam of length L subjected to point force, $F\hat{z}$, at its center[43]

$$EI\frac{\partial^4 u}{\partial x^4} - T\frac{\partial^2 u}{\partial x^2} = \frac{F}{2}(-\delta(x) + 2\delta(x - L/2) - \delta(x - L)) \tag{2}$$

where $u(x)$ is the transversal displacement in the z direction, x is the beam longitudinal axis, E is the effective Young's modulus, I is the area moment of inertia, and T is the overall tension along the wire. The first term originates from the beam bending, and the second term is attributed to initial tension and stretching along the axial direction of the beam. The overall tension is given by

$$T = T_0 + \frac{ES}{2L_{relx}}\int_0^L \left(\frac{\partial u}{\partial x}\right)^2 dx \tag{3}$$

where T_0 is the residual or initial tension, L_{relx} is the relaxed length of the beam (with zero strain), and L is the length of the beam between the two clamping points. The relaxed beam length may be smaller or larger than L, depending on whether the initial tension is positive or negative, respectively. However, a simple calculation shows that $L_{relx}/L = E/(E + \sigma_0)$, where $\sigma_0 = T_0/S$, and $S = \pi R^2$ is the circular beam cross section. In many experiments that use the three-point bending method, Young's modulus is much larger than σ_0 (by at least few hundreds), rendering the approximation $L_{relx} \approx L$ completely justified.

After integrating eq 2 with respect to x and assuming that $T > 0$ for the forthcoming analysis, the following analytical solution is found for the common boundary conditions of doubly clamped beam ($u(0) = u(L) = u'(0) = u'(L) = 0$):

$$u(x) = \frac{F}{2T}\frac{1}{\cosh(L/4L_0)}[x\cosh(L/4L_0) - L_0(\sinh(L/4L_0) - \sinh((L - 4x)/4L_0))] \tag{4}$$

where $L_0^2 = EI/T$. At $x = L/2$, eq 4 reduces to

$$u(L/2) = \frac{F}{2T}\frac{1}{\cosh(L/4L_0)}[(L/2\cosh(L/4L_0) - 2L_0\sinh(L/4L_0))] \tag{5}$$

Plugging eq 4 back into eq 3 yields

$$T = T_0 + \frac{ESF^2}{16T^2}\frac{1}{\cosh^2(L/4L_0)}[2 + \cosh(L/2L_0) - 6L_0/L\sinh(L/2L_0)] \tag{6}$$

For small deflections and low T_0, eq 5 may be expanded in powers of T to obtain

$$u(L/2) \approx \frac{FL^3}{192EI}\left(1 - \frac{L^2T}{40EI} + \frac{17}{26880}\left(\frac{L^2T}{EI}\right)^2\right) \tag{7}$$

The latter equation offers two main observations. First, we see that the relevant small parameter of the expansion is $\alpha = L^2T/EI = (L/L_0)^2$, which measures the ratio between the stretching and bending contributions to the beam deflection. Second, rewriting eq 7 in the following manner

$$F_{ext} \equiv F = \frac{192EI}{L^3}u(L/2)f(\alpha) \tag{8}$$

yields the well-known linear beam deflection approximation for $f(\alpha) = 1$. This relationship is commonly used in the literature to extract the Young's modulus of the beam.[26,29−32] The disadvantage of the linear model is that it is applicable only for deflections that are smaller than the beam's thickness and is extremely sensitive to initial stresses, as will be discussed below. For deflections greater or comparable to the beam's thickness (referred to as large deflections), tensile forces due to stretching become significant, and the force-deflection (F−D) curve deviates substantially from linearity. This can be described by adding a cubic term, giving only a rough approximation.[25]

It was only in 2006 that Heidelberg et al.[25] introduced a model consisting of a Padé approximation to the analytical solution of the beam equation that produces a F−D curve for the entire range of deflections. This model was further used only in subsequent work by co-workers.[28,33] In this study, we follow the analysis performed by Heidelberg et al.[25] and introduce also the exact set of equations and relevant approximations for the case of initial stresses.

The first step is to find $f(\alpha)$. Plugging eq 5 into eq 8 and eliminating F results in

$$f(\alpha) = \frac{\alpha}{48 - \frac{192\tanh(\sqrt{\alpha}/4)}{\sqrt{\alpha}}} \tag{9}$$

Inserting eqs 8 and 9 into eq 6 yields

$$\left(\alpha - \frac{L^2T_0}{EI}\right)\frac{\cosh^2(\sqrt{\alpha}/4)}{2 + \cosh(\sqrt{\alpha}/2) - 6\sinh(\sqrt{\alpha}/2)/\sqrt{\alpha}}(1 - 4\tanh(\sqrt{\alpha}/4)/\sqrt{\alpha})^2 = \frac{S}{I}u^2(L/2) \tag{10}$$

For a given set of F−D data, eqs 8 and 10 are solved self-consistently, thus finding the two unknowns, E and T_0. This procedure is very slow to converge, and if the residual tension is negative, which is quite common, the obtained result might be wrong, depending on the initial guess for the two unknown variables. To facilitate this procedure and to develop better intuition regarding the beam deflections, various approximations may be applied. In Yaish et al.[44] we present a detailed theoretical analysis that compares different approximations for the F−D curve. The final conclusion was for displacements that are up to 10 times the NW radius, E and T_0 can be extracted

DOI: 10.1021/nl5047939
Nano Lett. XXXX, XXX, XXX−XXX

with excellent agreement (less than 2% difference) by fitting the F−D data to eq 8 using the following approximation:

$$f_{app}(\alpha_{app}) = 1 + 2.412\cdot10^{-2}\alpha_{app} - 1.407\cdot10^{-6}\alpha_{app}^{\ 2} \quad (11)$$

where

$$\alpha_{app} \equiv \frac{L^2 T_0}{EI} + \frac{6\epsilon(140+\epsilon)}{350+3\epsilon} \quad (12)$$

and $\epsilon = u^2 S/I$. These equations are valid for both elongation ($T_0 > 0$) as well as compression ($T_0 < 0$) residual stresses.

The resulting E_{eff} is the effective Young's modulus of the composite structure that comprises a Si core and a SiO_2 shell. The flexural rigidity of a core−shell system is given by[45]

$$E_{eff}I_{eff} = E_{core}I_{core} + E_{shell}I_{shell} \quad (13)$$

where I is the area moment of inertia (which is $\pi r^4/4$ for a cylinder and $\pi(r_{outer}^{\ 4} - r_{inner}^{\ 4})/4$ for a cylindrical shell) and $E_{core(shell)}$ is the Young's modulus of the core(shell). Together, the following relationship for the effective modulus is derived:[46]

$$E_{eff} = E_{shell} + (E_{core} - E_{shell})\left(\frac{d_{core}}{d_{total}}\right)^4 \quad (14)$$

where E_{shell} = 70 GPa,[47] and d_{core} (d_{total}) is the NW core (total) diameter. The circular cross sections were verified by high resolution scanning electron microscopy and high resolution transmission electron microscopy images of several typical wires. Surprisingly, the relative strength of the stretching and bending rigidities, represented by α, is very similar (within 10%) for the two common circular and hexagonal cross sections, and as a result, the Young's modulus and residual stresses extracted from the experimental data for these two cases are very close.

Equipped with the theoretical model and the fitting procedure, the effective Young's modulus and the residual tension may be extracted from the experimental curves. Figure 3 depicts two fitting curves for the experimental data, obtained by the analytical model (eqs 8 and 11), including and not including the initial stress along the beam (red and green curves, respectively). The fitting results are E_{eff} = 140 GPa, which corresponds to E_{Si} = 193 GPa with a 2 nm oxide sheath according to the core−shell model (eq 14), and σ_0 = 96 MPa; the stress-free model yields E_{eff} = 160 GPa, which corresponds to E_{Si} = 230 GPa.

The calculated Young's modulus for the core is in excellent agreement with bulk Si in the ⟨111⟩ direction ($E_{\langle111\rangle}$ = 190 GPa), a result that is expected considering the NWs used.[48] The high result obtained for the stress-free case does not agree with Si elastic moduli, and the fitting quality is lower than for the nonzero σ_0 case. This result emphasizes the importance of including the residual stress in the model, in comparison with the stress-free case.

Figure 6a depicts the resulting E_{eff} (black circles) for our three-point bending experiments conducted on nine SiNW devices. Seven devices had native oxide ($d_{shell} \approx 2$ nm) and two were oxidized ($d_{shell} \approx 7$ nm). These results were compared with the core−shell model introduced by eq 14. This model, however, offers four relevant possibilities for our study: two shell thicknesses (2 and 7 nm) and two expected core Young's moduli, E_{core} ($E_{\langle110\rangle,\langle112\rangle}$ = 170 GPa, and $E_{\langle111\rangle}$ = 190 GPa). The red and magenta continuous lines correspond to unoxidized SiNWs with E_{core} = 170 and 190 GPa, respectively,

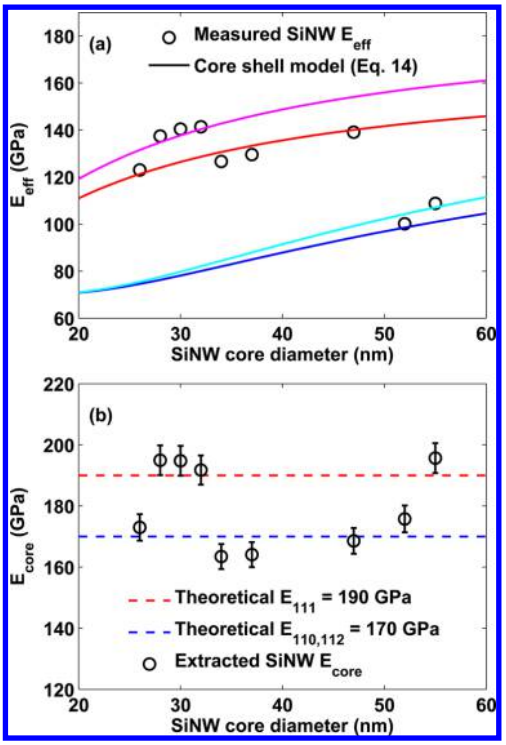

Figure 6. (a) Core−shell model prediction with E_{core} = 170 or 190 GPa, 2 or 7 nm shell, and E_{shell} = 70 GPa (solid colored lines, see main text) alongside the extracted fitting results for the effective Young's modulus (black circles). (b) Core Young's modulus calculated according to the core−shell model from the fitting results (black circles). The colored dashed lines correspond to $E_{\langle110\rangle,\langle112\rangle}$ = 170 GPa and $E_{\langle111\rangle}$ = 190 GPa.

while the blue and light blue lines represent oxidized wires with E_{core} = 170 and 190 GPa, respectively. Note the good agreement between the theoretical model and the measured data, and the dependence of E_{eff} on the NW diameter, as predicted. Figure 6b shows the resulting E_{core} vs NW diameter (black circles). The colored dashed lines correspond to the theoretical bulk values of the Young's moduli of silicon. The experimental data are scattered nicely along these two dashed lines, confirming our previous knowledge that these SiNWs have ⟨110⟩, ⟨112⟩, and ⟨111⟩ crystallographic growth orientation. The average Young's moduli obtained from these devices are 169 ± 10 and 194 ± 12 GPa, respectively. These results are in good agreement with the theoretical values of 170 and 190 GPa. Interestingly, the residual stress for these NWs ranges between −30 and 450 MPa, with no obvious correlation between NW diameters and stress.

The resulting residual stress can also be modified after device fabrication. This possibility is essential for tuning the electrical properties of the wire to achieve optimal operation. One method is attributed to RTA, as presented in Figure 4. Fitting results before RTA treatment are E_{eff} = 123 GPa and σ_0 = 159 MPa, which corresponds to E_{core} = 173 GPa, while after RTA treatment E_{eff} = 113 GPa and σ_0 = 45 MPa, yielding E_{core} = 154 GPa.

E_{eff} is smaller since NiSi Young's modulus is smaller than Si Young's modulus (reported to be about 130 GPa[49]) and because parts of the SiNW turn into NiSi during RTA. A significant change of about −115 MPa in the initial stress was found, corresponding to compression during RTA. This result is expected since the unit cells of the various silicide phases are

DOI: 10.1021/nl5047939
Nano Lett. XXXX, XXX, XXX−XXX

bigger than the silicon unit cell, thus elongating the NW and reducing the original positive strain.

In conclusion, three-point bending experiments were performed on fabricated doubly clamped SiNW beams of two oxide sheath thicknesses, before and after RTA. An analytical model was used to extract the Young's modulus and the initial stress for these wires. Excellent agreement was found between the extracted Young's moduli of these SiNWs and the predicted values for bulk silicon based on the NW crystallographic growth orientation. This analysis supports the core−shell model in that it properly describes the elastic properties of SiNWs with diameters above 20 nm and may be used as a postfabrication characterization tool for NW crystal orientation.

RTA was found to cause axial compressive stress within the SiNW, to such extent that some devices experienced Euler−Bernoulli buckling instability and formed arched beams. Further research is needed to analyze the mechanical properties of these arched devices.

AUTHOR INFORMATION

Corresponding Author

*E-mail: yuvaly@ee.technion.ac.il.

Notes

The authors declare no competing financial interest.

ACKNOWLEDGMENTS

The authors wish to thank Dr. G. M. Cohen for assistance, Dr. A. Lahav and Dr. M. Drozdov for TEM imaging, and Dr. M. Beregovsky for useful discussion. We also thank the Russell Berrie Nanotechnology Institute, the Micro Nano Fabrication Unit at the Technion, and the Ministry of Industry, Trade and Labor via the MAGNET program (ALPHA consortium) for their support.

REFERENCES

(1) Cui, Y.; Zhong, Z.; Wang, D.; Wang, W. U.; Lieber, C. M. *Nano Lett.* **2003**, *3*, 149−152.

(2) Zheng, G.; Lu, W.; Jin, S.; Lieber, C. M. *Adv. Mater.* **2004**, *16*, 1890−1893.

(3) Kim, D.; Jung, Y.; Park, M.; Kim, B.; Hong, S.; Choi, M.; Kang, M.; Yu, Y.; Whang, D.; Hwang, S. *IEEE Trans. Nanotechnol.* **2008**, *7*, 683−687.

(4) Feng, X. L.; He, R.; Yang, P.; Roukes, M. L. *Nano Lett.* **2007**, *7*, 1953−1959.

(5) Li, Q.; Koo, S.-M.; Richter, C.; Edelstein, M.; Bonevich, J.; Kopanski, J.; Suehle, J.; Vogel, E. *IEEE Trans. Nanotechnol.* **2007**, *6*, 256−262.

(6) Li, M.; Bhiladvala, R. B.; Morrow, T. J.; Sioss, J. A.; Lew, K.-K.; Redwing, J. M.; Keating, C. D.; Mayer, T. S. *Nat. Nanotechnol.* **2008**, *3*, 88−92.

(7) Cui, Y.; Wei, Q.; Park, H.; Lieber, C. M. *Science* **2001**, *293*, 1289−1292.

(8) Kim, K. S.; Lee, H.-S.; Yang, J.-A.; Jo, M.-H.; Hahn, S. K. *Nanotechnology* **2009**, *20*, 235501.

(9) Bunimovich, Y. L.; Shin, Y. S.; Yeo, W.-S.; Amori, M.; Kwong, G.; Heath, J. R. *J. Am. Chem. Soc.* **2006**, *128*, 16323−16331.

(10) He, R.; Yang, P. *Nat. Nanotechnol.* **2006**, *1*, 42−46.

(11) Thompson, S.; Sun, G.; Choi, Y. S.; Nishida, T. *IEEE Trans. Electron. Dev. Lett.* **2006**, *53*, 1010−1020.

(12) Fan, X. F.; Register, L. F.; Winstead, B.; Foisy, M. C.; Chen, W.; Zheng, X.; Ghosh, B.; Banerjee, S. K. *IEEE Trans. Electron. Dev.* **2007**, *52*, 291−296.

(13) Chang, W.; Lin, J. *Microelectron. Eng.* **2009**, *86*, 1965−1968.

(14) Yu, M.-F.; Lourie, O.; Dyer, M. J.; Moloni, K.; Kelly, T. F.; Ruoff, R. S. *Science* **2000**, *287*, 637−640.

(15) Hoffmann, S.; Utke, I.; Moser, B.; Michler, J.; Christiansen, S. H.; Schmidt, V.; Senz, S.; Werner, P.; Gosele, U.; Ballif, C. *Nano Lett.* **2006**, *6*, 622−625.

(16) Lu, K.-C.; Wu, W.-W.; Wu, H.-W.; Tanner, C. M.; Chang, J. P.; Chen, L. J.; Tu, K. N. *Nano Lett.* **2007**, *7*, 2389−2394.

(17) Hsin, C.-L.; Mai, W.; Gu, Y.; Gao, Y.; Huang, C.-T.; Liu, Y.; Chen, L.-J.; Wang, Z.-L. *Adv. Mater.* **2008**, *20*, 3919−3923.

(18) Zhu, Y.; Xu, F.; Qin, Q.; Fung, W.; Lu, W. *Nano Lett.* **2009**, *9*, 3934−3939.

(19) Xu, F.; Lu, W.; Zhu, Y. *ACS Nano* **2011**, *5* (1), 672−678.

(20) Smith, D. A.; Holmberg, V. C.; Korgel, B. A. *ACS Nano* **2010**, *4* (4), 2356−2362.

(21) Li, X.; Gao, H.; Murphy, C. J.; Caswell, K. K. *Nano Lett.* **2003**, *3*, 1495−1498.

(22) Riaz, M.; Nur, O.; Willander, M.; Klason, P. *Appl. Phys. Lett.* **2008**, *92*, 103118.

(23) Tabib-Azar, M.; Nassirou, M.; Wang, R.; Sharma, S.; Kamins, T. I.; Islam, M. S.; Williams, R. S. *Appl. Phys. Lett.* **2005**, *87*, 113102.

(24) Wong, E. W.; Sheehan, P. E.; Lieber, C. M. *Science* **1997**, *277*, 1971−1975.

(25) Heidelberg, A.; Ngo, L. T.; Wu, B.; Phillips, M. A.; Sharma, S.; Kamins, T. I.; Sader, J. E.; Boland, J. J. *Nano Lett.* **2006**, *6*, 1101−1106.

(26) Paulo, A. S.; Bokor, J.; Howe, R. T.; He, R.; Yang, P.; Gao, D.; Carraro, C.; Maboudian, R. *Appl. Phys. Lett.* **2005**, *87*, 053111.

(27) Wu, B.; Heidelberg, A.; Boland, J. J. *Nat. Mater.* **2005**, *4*, 525−529.

(28) Ngo, L. T.; Almecija, D.; Sader, J. E.; Daly, B.; Petkov, N.; Holmes, J. D.; Erts, D.; Boland, J. J. *Nano Lett.* **2006**, *6*, 2964−2968.

(29) Jing, G. Y.; Duan, H. L.; Sun, X. M.; Zhang, Z. S.; Xu, J.; Li, Y. D.; Wang, J. X.; Yu, D. P. *Phys. Rev. B* **2006**, *73*, 235409.

(30) Xiong, Q.; Duarte, N.; Tadigadapa, S.; Eklund, P. C. *Nano Lett.* **2006**, *6*, 1904−1909.

(31) Varghese, B.; Zhang, Y.; Dai, L.; Tan, V. B. C.; Lim, C. T.; Sow, C.-H. *Nano Lett.* **2008**, *8*, 3226−3232.

(32) Ni, H.; Li, X.; Gao, H. *Appl. Phys. Lett.* **2006**, *88*, 043108.

(33) Wen, B.; Sader, J. E.; Boland, J. J. *Phys. Rev. Lett.* **2008**, *101*, 175502.

(34) Almecija, D.; Blond, D.; Sader, J. E.; Coleman, J. N.; Boland, J. J. *Carbon* **2009**, *47*, 2253−2258.

(35) Shirak, O.; Shtempluck, O.; Kotchtakov, V.; Bahir, G.; Yaish, Y. *Nanotechnology* **2012**, *23*, 395202.

(36) Zhou, P.; Wu, C.; Li, X. *Meas. Sci. Technol.* **2008**, *19*, 115703.

(37) Weber, W. M.; Geelhaar, L.; Graham, A. P.; Unger, E.; Duesberg, G. S.; Liebau, M.; Pamler, W.; Cheze, C.; Riechert, H.; Lugli, P.; Kreupl, F. *Nano Lett.* **2006**, *6*, 2660−2666.

(38) Weber, W. M.; Geelhaar, L.; Unger, E.; Chze, C.; Kreupl, F.; Riechert, H.; Lugli, P. *Phys. Status Solidi B* **2007**, *244*, 4170−4175.

(39) Byon, K.; Tham, D.; Fischer, J. E.; Johnson, A. T. *Appl. Phys. Lett.* **2007**, *90*, 143513.

(40) Yaish, E. Y.; Katsman, A.; Cohen, G. M.; Beregovsky, M. *J. Appl. Phys.* **2011**, *109*, 094303.

(41) Beregovsky, M. J.; Katsman, A.; Hajaj, E. M.; Yaish, E. Y.; Beregovsky, M. J.; Katsman, A.; Hajaj, E. M.; Yaish, E. Y. *Solid-State Electron.* **2013**, *80*, 110.

(42) Calahorra, Y.; Yaish, Y. E. in preparation 2015.

(43) Landau, L.; Lifshitz, E. *Theory of Elasticity*, 3rd ed.; Pergamon Press: Oxford, U.K., 1986.

(44) Yaish, E. Y.; Calahorra, Y.; Shtempluck, O.; Kotchtakov, V. *J. Appl. Phys.* **2015** (in press).

(45) Chen, C. Q.; Shi, Y.; Zhang, Y. S.; Zhu, J.; Yan, Y. J. *Phys. Rev. Lett.* **2006**, *96*, 075505.

(46) Gordon, M. J.; Baron, T.; Dhalluin, F.; Gentile, P.; Ferret, P. *Nano Lett.* **2009**, *9*, 525−529.

(47) Hai, N.; Li, X.; Gao, H. *Appl. Phys. Lett.* **2006**, *88*, 043108−043108.

(48) According to SiNWs supplier, growth wafers bear SiNWs of ⟨110⟩, ⟨112⟩, and ⟨111⟩ directions. Anisotropic crystals have different Young's modulus in different directions given by $(1/E) = S_{11} - 2(S_{11} - S_{12} - (1/2)S_{44})(l_1^2l_2^2 + l_2^2l_3^2 + l_1^2l_3^2)$,[50] where (l_1,l_2,l_2) are

DOI: 10.1021/nl5047939
Nano Lett. XXXX, XXX, XXX−XXX

the directional cosines of the crystal direction. Yielding $E_{110} = E_{112} =$ 170 GPa and $E_{111} = 190$ GPa.
(49) Qin, M.; Poon, V. M. C. *J. Mater. Sci.* **2000**, *19*, 2243−2245.
(50) Senturia, S. D. *Microsystem Design*; Kluwer Academic Publishing: Dordrecht, the Netherlands, 2001.

DOI: 10.1021/nl5047939
Nano Lett. XXXX, XXX, XXX−XXX